

# Earthquakes and slip rate of the southern Sagaing fault: insights from an offset ancient fort wall, lower Burma (Myanmar)

Yu Wang,<sup>1</sup> Kerry Sieh,<sup>2</sup> Thura Aung,<sup>3</sup> Soe Min,<sup>4</sup> Saw Ngwe Khaing<sup>4</sup> and Soe Thura Tun<sup>3</sup>

<sup>1</sup>Tectonics Observatory, California Institute of Technology, Pasadena, USA. E-mail: wangyu79@gps.caltech.edu

<sup>2</sup>Earth Observatory of Singapore, Nanyang Technological University, Singapore

<sup>3</sup>Myanmar Earthquake Committee, Myanmar Engineering Society, Myanmar

<sup>4</sup>Department of Geology, Yangon University, Myanmar

Accepted 2010 December 9. Received 2010 November 18; in original form 2010 July 19

## SUMMARY

Field investigations of an ancient fortress wall in southern Myanmar reveal an offset of ~6 m across the Sagaing fault, the major right-lateral fault between the Sunda and Burma plates. The fault slip rate implied by offset of this 16th-century fortress is between 11 and 18 cm yr<sup>-1</sup>. A palaeoseismological excavation within the fortress reveals at least two major fault ruptures since its construction. The slip rate we obtained is comparable to geodetic and geological estimates farther north, but is only 50 per cent of the spreading rate (38 mm yr<sup>-1</sup>) at the Andaman Sea spreading centre. This disparity suggests that other structures may be accommodating deformation within the Burma Plate. We propose two fault-slip scenarios to explain the earthquake-rupture history of the southern Sagaing fault. Using both small offset features along the fault trace and historical records, we speculate that the southern Sagaing fault exhibits a uniform-fault-slip behaviour and that one section of the fault could generate a *M*7+ earthquake within the next few decades.

**Key words:** Palaeoseismology; Transform faults; Neotectonics; Asia.

## 1 INTRODUCTION

The long, partially preserved record of civilization in Myanmar (Burma) provides an unusual opportunity to understand the recent behaviour of some of its active faults. In particular, inscriptions on some Buddhist religious shrines (pagodas) record damages and renovations through about the past 2000 years (Win Swe 2006). These could give palaeoseismologists a great advantage in determining the timing and recurrence intervals of historical earthquakes, especially if they can determine the seismic sources for these historical events.

Thus, we initiated palaeoseismic work in Myanmar with the hope that the precise timing of pagoda destructions would provide exceptional constraints on the recurrence characteristics of large seismic events on the 1200-km-long strike-slip Sagaing fault.

The Sagaing fault is one of the great strike-slip faults of Southeast Asia, bisecting Myanmar from north to south (Fig. 1a; Curray *et al.* 1979; Le Dain *et al.* 1984). The fault is the principal right-lateral boundary between the Sunda and Burma plates (Curray *et al.* 1979; Bird 2003; Curray 2005). Its southern terminus is at the Andaman Sea spreading system, and its northern end fans out towards the Eastern Himalayan syntaxis (Curray 2005). Like the San Andreas fault in California but in contrast to the great Sumatran fault in Indonesia (Sieh & Natawidjaja 2000), its trace is remarkably smooth

and continuous (Le Dain *et al.* 1984). This smooth geometry likely reflects very large total offsets.

Brown and Chhibber (Brown *et al.* 1931; Brown & Leicester 1933; Chhibber 1934) were the first to write about the Sagaing fault. It was the alignment of several moderate to strong earthquakes from southern to northcentral Myanmar in the early 20th century that attracted their attention and led them to suggest the existence of a long active fault cutting across the active fluvial plains of central Burma. Nonetheless, the fault trace itself was not recognized and mapped until decades later (Win Swe 1970). This initial delineation of the fault trace was based on field mapping guided by aerial photography. Subsequently more details of its geometry have been revealed through various field investigations and remote sensing studies (Le Dain *et al.* 1984; Myint Thein *et al.* 1991; Replumaz 1999; Tsutsumi & Sato 2009).

The proximity of the Sagaing fault to several major cities and towns means that large numbers of people are at risk. In the south these cities include the Myanmar's new capital, Nay Pyi Daw, and the ancient capitals of Taungoo and Bago (previously called Pegu). Yangon, the biggest city and largest economic centre in Myanmar, and until recently the country's capital, is only 36 km west of the fault trace. These cities have suffered significant seismic damage within the past millennium (Thawbita 1976). The high degree of

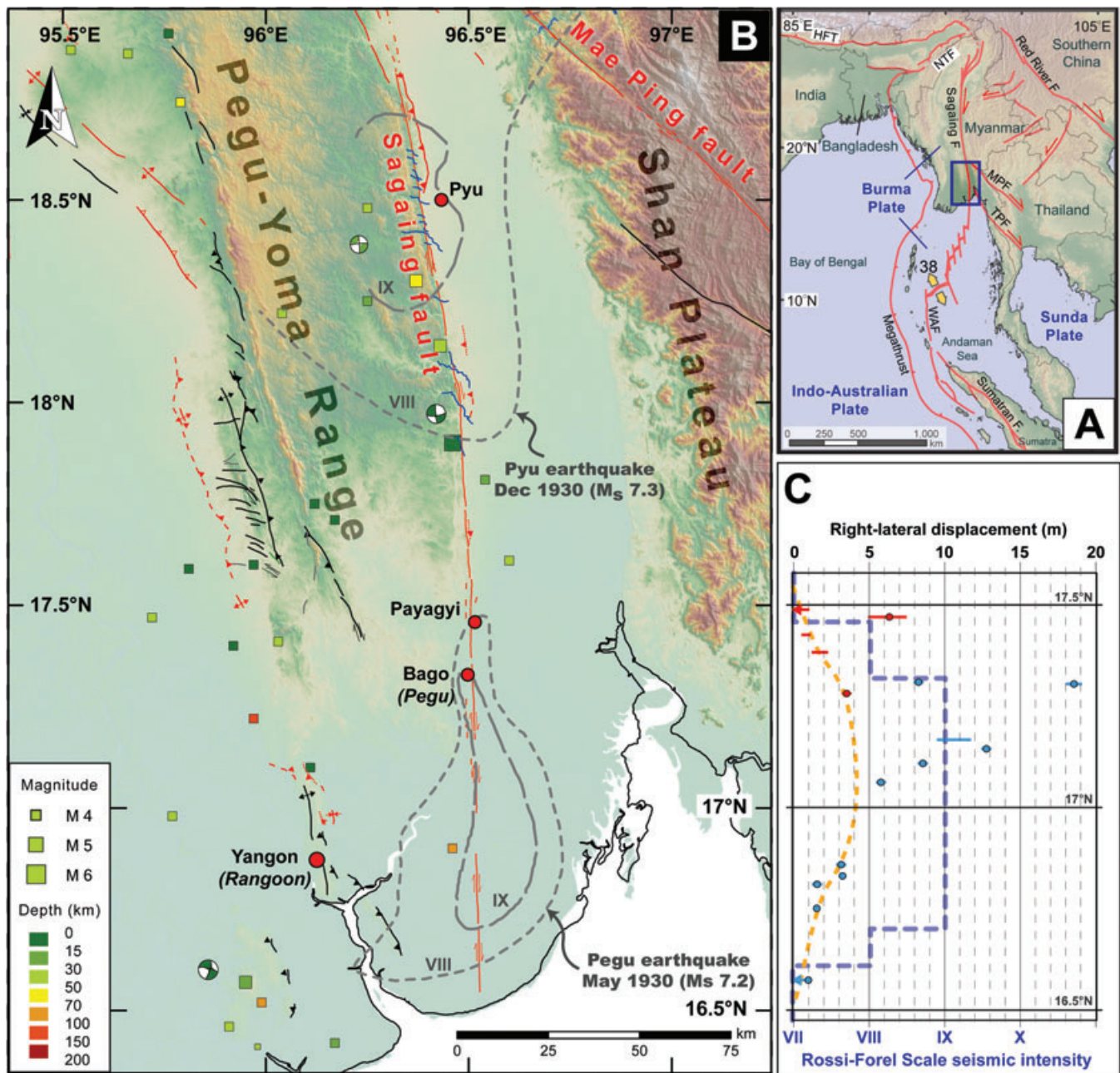


**Figure 1.** Active tectonic framework and recent earthquake history of southcentral Myanmar (Burma). (a) Myanmar is currently experiencing strain partitioning between the Indian and Sunda plates. In the west the Indian Plate is colliding obliquely with the Burma Plate along the northern extension of the Sunda megathrust (Socquet *et al.* 2006). In the east, relative motion between the Burma and Sunda plates occurs along the 1200-km-long Sagaing fault. Farther south, this relative motion rifts the Andaman Sea Basin and bisects Sumatra along the 1900-km-long Sumatran fault (Sieh & Natawidjaja 2000) and West Andaman fault (Berglar *et al.* 2010). Red lines represent major tectonic faults (after Tapponnier *et al.* 1982; Lacassin *et al.* 1997; Lacassin *et al.* 1998). Arrows indicate their sense of slip. Orange arrows show the rifting direction of the Andaman Sea spreading centre; Spreading rate ( $\text{mm yr}^{-1}$ ) is from Kamesh Raju *et al.* (2004). HFT, Himalayan Frontal Thrust; NTE, Naga thrust fault; MPF, Mae Ping fault; TPF, Three Pagodas fault; WAF, West Andaman fault. Blue box shows the map area of (b). (b) Active structures of southcentral Myanmar. Active structures are red. Blue lines indicate large offset stream channels. Coloured squares are background seismicity from the USGS/NEIC global earthquake catalogue since 1973. Focal mechanisms are from the Global CMT Catalogue since 1976. Grey dashed lines delimit high seismic intensities during the 1930 May Pegu earthquake and 1930 December Pyu earthquake (Brown *et al.* 1931; Brown & Leicester 1933). (c) Right-lateral displacements along the part of the southern Sagaing fault that bisects the high-intensity region of the 1930 May Pegu earthquake. Blue dots are measurements from Tsutsumi & Sato (2009). Red dots are our measurements. Horizontal bars show estimated uncertainty of each measurement. Yellow dashed line represents the inferred slip distribution during the 1930 May Pegu earthquake as judged from the smallest right-lateral displacements measured in the field. Blue dashed line, which indicates the distribution of seismic intensity of the Pegu earthquake (Brown *et al.* 1931), shows good correlation with the inferred coseismic slip distribution.

activity of the fault and its proximity to large populations makes the southern reach of the Sagaing fault a prime target for modern neotectonic, palaeoseismologic, seismologic and geodetic study.

Another important aspect of the Sagaing fault is its slip rate. Estimates vary by a factor of 2. Curray *et al.* (1982) inferred a long-term slip rate of  $35.4 \text{ mm yr}^{-1}$ , based upon spreading of 460 km in 13 Ma across the Andaman Sea spreading centre. Myint Thein *et al.* (1991) suggested just half that value,  $18.5 \text{ mm yr}^{-1}$ , assuming a later (11 Ma) initiation of rifting and a 203 km offset of a metamorphic belt near Mandalay. Bertrand *et al.* (1998) calculated a slip rate of between  $10 \pm 1$  and  $23 \pm 3 \text{ mm yr}^{-1}$ , from a 2.7 to 6.5 km offset of a 0.25 to 0.31 Myr old basalt flow in central Myanmar. Vigny *et al.* (2003) used 2 yr of GPS observations to estimate  $18 \text{ mm yr}^{-1}$  of elastic deformation across the central Sagaing fault. Meade (2007) estimated the rate using GPS observations in a block model for the Indian and Southeast Asian plates. His model suggests that the strike-slip rate between the Indian and Southeast Asian Plate is 17 and  $49 \text{ mm yr}^{-1}$  at across the central and northern Sagaing fault, respectively. His estimation represents the maximum value for the Sagaing fault if all of the strike-slip motions between the Indian and Southeast Asian Plate are concentrated along this single fault. Liu & Bird (2008) predicted a rate of  $22\text{--}35 \text{ mm yr}^{-1}$  on the Sagaing fault by using their kinematic model to fit the regional geodetic velocities, geological fault slip rates and stress directions.

Comparison of these slip-rate estimates shows that estimates for the central Sagaing fault (Myint Thein *et al.* 1991; Bertrand *et al.* 1998; Vigny *et al.* 2003) are slower than estimates from simplified tectonic models (Curray *et al.* 1982; Meade 2007; Liu & Bird 2008), even if these models consider the slip partitioning between Indo-Burma Range and Sagaing fault (Liu & Bird 2008). Also, the rate seems to vary geographically. Rates across the central Sagaing fault are slower than the Andaman Sea spreading rate (Curray *et al.* 1982; Kamesh Raju *et al.* 2004). This ostensible northward decrease in rate implies that about  $2 \text{ cm yr}^{-1}$  of the opening rate across the Andaman Sea spreading centre has been partitioned between the Sagaing fault and one or more other structures.

In this study, we reconstruct the offset and estimate the construction date of an ancient fortress, thereby enabling an evaluation of both the earthquake history and slip rate of the southern Sagaing fault. We further refine the fault's recent history through a palaeoseismological study within the fortress. This rate, averaged over just a few centuries, fills a gap in rates between geological rates averaged over more than a million years and geodetic rates spanning just a few years.

## 2 ACTIVE TECTONICS OF THE SOUTHERN SAGAING FAULT AND SURROUNDING AREA

### 2.1 Structural overview of southern Myanmar

Fig. 1(b) shows active tectonic features in southern Myanmar. This map includes primarily tectonic geomorphologic features deduced from analysis of 90-m-resolution SRTM and 15-m stereo ASTER VNIR images. Aerial photography at 1:25 000 and 1:50 000 scales also aided in our mapping along the western and eastern flanks of the Pegu-Yoma range.

The distribution of active structures indicates that tectonic strain is accommodated not only by the Sagaing fault, but also by other structures in southern Myanmar. These active structures occur in three regions. The western and eastern edges of the Pegu-Yoma range and the western Shan plateau.

Along the western edge of the Pegu-Yoma range, west-facing scarps and slightly warped lateritic terraces suggest the existence of active contractional structures. These structures are mostly NNW trending, oblique to the orientation of regional compressional stress (Gahalaut & Gahalaut 2007), as would be expected in a transpressional regime. The lack of active strike-slip structures along the western side of the Pegu-Yoma range suggests that mostly contraction perpendicular to the Sagaing fault is occurring there.

On the other side of the Sagaing fault, on the western Shan plateau, offset drainages along the major intraplate Mae Ping fault (Morley 2002) suggest recent strike-slip activity. Clear geomorphic evidence of recent activity occurs only along that section of the Mae Ping fault closest to the Sagaing fault. The youthful geomorphic expression of the Mae Ping fault implies that the Sagaing fault is not the only locus of strike-slip motion, and that strain partitioning is not as simple as it appears to be farther south, in Sumatra (Fitch 1972; McCaffrey 1991; Genrich *et al.* 2000; Sieh & Natawidjaja 2000; Chlieh *et al.* 2007).

### 2.2 Southern Sagaing fault

The southern Sagaing fault shows clear evidence of right-lateral offset, along the eastern edge of the Pegu-Yoma range. The fault forms a remarkably straight boundary between the Miocene-to-Pleistocene sediments of the Pegu-Yoma range and Holocene sediments of the fluvial plain. South of  $18.5^\circ\text{N}$ , the fault's geomorphology varies markedly along strike. Between  $18.5^\circ\text{N}$  and  $17.5^\circ\text{N}$ , well-aligned offset stream channels, linear valleys and linear scarps dominate. Right-lateral channel separations range from  $\sim 500 \text{ m}$  to  $4 \text{ km}$ . The length of these separations implies a long history of offset recorded by the landforms. South of  $17.5^\circ\text{N}$ , the fault trace traverses predominantly the active fluvial plain of the Sittaung and Bago Rivers, whose deltas are still prograding southward. Meandering river landforms dominate tectonic landforms. In this region of very low and young topographical relief, the Sagaing fault's trace is marked intermittently by small west-facing scarps and N-S trending tectonic ridges. The rapid construction of this fluvial landscape and the fact that fluvial features are nearly parallel to tectonic landforms make it difficult to identify clear tectonic landforms.

The trace of the Sagaing fault changes strike by about  $10^\circ$  at  $18^\circ\text{N}$ . This sharp kink results in a local *transpressional* environment, as evidenced by minor contraction structures on the eastern fluvial plain.

The NEIC/USGS global earthquake catalogue (magnitudes greater than 4 since 1973) shows a non-uniform distribution of background seismicity along the southern Sagaing fault. Epicentres cluster around the kink at  $18^\circ\text{N}$ . Global CMT solutions suggest that the fault plane strikes  $\sim 355^\circ$  south of and  $335^\circ$  north of the fault bend, which is consistent with the change of fault orientation at the surface. Moderate earthquakes north and south of the kink are rare in the catalogue; thus the cluster of recent activity may mark highly coupled sections to the north and south.

### 2.3 1930 May Pegu earthquake and 1930 December Pyu earthquake

Two major earthquakes occurred in rapid succession along the southern Sagaing fault in the 20th century. The Pegu earthquake, which shook the region violently on 1930 May 5, had an estimated magnitude ( $M_s$ ) of 7.2 (Pacheco & Sykes 1992). The Pyu earthquake, which occurred just 6 months later on 1930 December 3, had a similar magnitude ( $M_s$  7.3), but was most severe farther

north. Grey dashed lines in Fig. 1(b) surround the regions of highest intensity (*Rossi-Forel* VIII–IX; Brown *et al.* 1931; Brown & Leicester 1933). This corresponds to Modified Mercalli intensities of VII–IX (Wood & Neumann 1931).

For both earthquakes, *Rossi-Forel* intensity IX extends about 60 km along the Sagaing fault. The *Rossi-Forel* intensity VIII zones are also parallel to the trend of the fault. The southern (Pegu) earthquake has a smaller and narrower region of intensity VIII than the northern (Pyu) earthquake. Also, the northern and southern terminations of the intensity VII zone are close to the edge of intensity-IX zone, which shows the rapid northward and southward decaying of the seismic intensity during the Pegu earthquake.

Study of recent earthquakes suggests the distribution of Modified Mercalli intensities >VIII coincides with the length of the seismic surface rupture (i.e. Sokolov & Wald 2002). Hence, we believe the high intensities of the Pegu and Pyu earthquakes likely represent the maximum lengths of their fault ruptures.

Although most of the southern Sagaing fault experienced high intensities during these two events, a section of lower intensity exists between 17.5°N and 18°N. This implies that at least a 50-km section of the fault between the two events of 1930 did not rupture during either of these two earthquakes.

## 2.4 Offsets along the Pegu section

From 2008 April to 2009 March, we conducted a series of field investigations to map the trace of the southern Sagaing fault and the possible surface rupture during the Pegu earthquake. We focused on the area between 17.5°N and 17.2°N, where the intensity of the Pegu earthquake decreased dramatically northward. Along this section, we also tried to collect stories of the earthquake in every village along the fault trace to determine whether or not offsets we found in the field formed during the earthquake. The interview records and field photos are included in the Supporting Information (Tables S1 and S2). Our work was a complement to that of Tsutsumi & Sato (2009), who conducted a similar survey farther south (from 17.2°N to 16.5°N). Our and their work allows us to make a more complete interpretation of slip during the Pegu earthquake of 1930.

Fig. 1(c) shows measurements of small dextral offsets along the southern Sagaing fault, deduced from our combined field observations. The *y*-axis spans ~100 km of the Sagaing fault that experienced high seismic intensities during the Pegu earthquake. Measured offsets range from ~20 m to less than 1 m. The lack of large offsets south of ~17°N likely reflect the southward-decreasing age of the southward-prograding fluvial plain. Local minimum offset values form a bell-shaped distribution centred at ~17°N. This distribution is comparable in form to the pattern of the seismic intensity along the fault during the Pegu earthquake. Therefore, we suggest that these horizontal offsets are coincident with the Pegu earthquake, the most recent large earthquake in the region.

## 3 OFFSET ANCIENT STRUCTURE

### 3.1 The Payagyi ancient fortress

15-metre resolution ASTER visible and near infrared (VNIR) imagery and 1:25 000 aerial photos show that the Sagaing fault cuts through a rectangular earthen embankment west of Payagyi, 16 km north of Bago (Fig. 2a). The age and offset of this man-made feature offers a great opportunity to constrain the fault slip rate along the

Pegu section of the Sagaing Fault. Tsutsumi & Sato (2009) also documented this offset ancient structure, but they were unable to measure the amount of displacement directly in the field.

There is no direct historical evidence that clarifies the function and the age of this feature. However, circumstantial evidence suggests it is either a fortress/stockade, or the temporary palace for royal usage. If the rectangular embankment is a military fortress (the standard military device for attackers and defenders in the history of Myanmar), then its construction could have occurred during 15th to 17th century. This was time of great military activity in the region, and Pegu (Bago) was wealthy enough to build outlying defences such as this one. It is also possible that the structure was built in mid-18th century, when Pegu was besieged, before being conquered by the Burmese King Alaungpaya in 1755–1757 (Harvey 1925). Both offensive and defensive sides built more than 40 stockades at that time, but mainly south of Pegu (Bago). Since there was also a second Alaungpaya army advancing from Taungoo in the north, this structure might have been built to defend Pegu from this northern troop.

Alternatively, the embankment might have served as a temporary palace to guard their religious treasures, built in 1574 or 1576, during the construction/renovation of the Payagyi Pagoda, 1.5 km to the east. The construction of a temporary palace is mentioned by U Kala, who wrote about Burmese history in the early 18th century. The English translation of his description is included in the Supporting Information (Table S3).

Archaeological materials found during our survey support, but do not prove, a 15th–16th-century date of construction. We found fragments of celadon pottery characteristic of 15th–16th-century Thai and Burmese ceramic production (Bob Hudson, field conversation, 2008) within the confines of the ancient structure. Although these fragments were found on the surface and were disturbed by the modern cultivation, they still suggest that there was human activity in this area in the 15th–16th centuries. It is reasonable to hypothesize that the construction of the embankment occurred then.

The trace of the fault is clearly demarcated geomorphologically from the northern wall through about the northern two thirds of the interior of the feature (Fig. 2b). The southern intersection of the fault trace and the fortress wall has been destroyed by construction of a modern E–W road.

The northern intersection is readily apparent in high-resolution satellite imagery and the 1:25 000 aerial photos, but it is difficult to estimate the right-lateral offset. The fault trace inside the ancient fortress wall aligns well with other tectonic features north and south of the fortress (Fig. 2b). Its northern extension corresponds to the western edge of a tectonically warped terrace, which blocks an eastward flowing stream, resulting in the creation of a sag-pond north of the fortress. The fault scarp is unclear near the southern fortress wall, but probably runs under the E–W running dirt-road. Farther south, the Sagaing fault is also unclear on the young flood-plain but probably corresponds to the western edge of a deformed terrace.

### 3.2 Estimation of offsets

In the summer of 2008 and spring of 2009, we used a total station to map the topography of the ancient fortress in order to estimate the offset of the northern fortress wall. Our survey allowed us to construct a 50-cm-resolution digital terrain model (DTM) within the fortress walls (Fig. 2c). This digital topography provides a crystal-clear image of not only the fault scarp south of the northern wall but

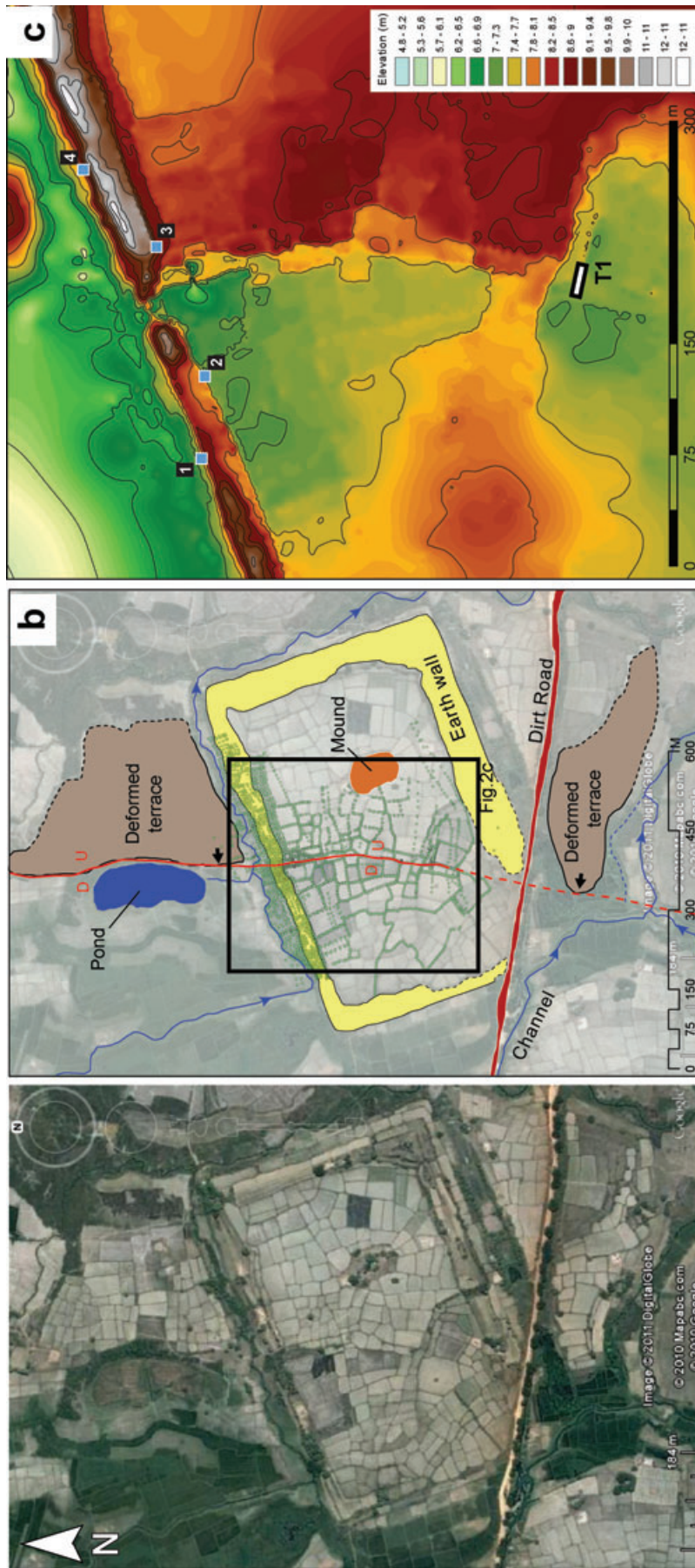


**Figure 2.** Landforms of the Payayyi ancient fortress, 16 km north of Bago. (a) Birds-eye view of the Payayyi ancient fortress from a Google Earth® image. The ancient fortress is at 17.480°N, 96.505°E and appears as a 650 m × 400 m rectangle amid rice paddies. (b) Geomorphologic interpretation from aerial photography and satellite imagery. Yellow depicts the fortress wall visible on the images. The vertical red line shows the trace of the Sagaing fault on the fluvial plain as revealed by field mapping and remote sensing. Black arrows indicate tectonic tilting of high terraces. Green dots are points surveyed by total station in spring 2009. The digital topography generated from the survey is in panel (c). (c) Digital terrain model (DTM) of part of the Payayyi ancient fortress. Grid cell size is 50 cm. The trace of the Sagaing fault is clear as a west-facing topographic scarp cutting across the middle of the map. Blue squares show the locations of pits dug through the base of the earthen fortress wall. T1 is the trench we dug across the fault.

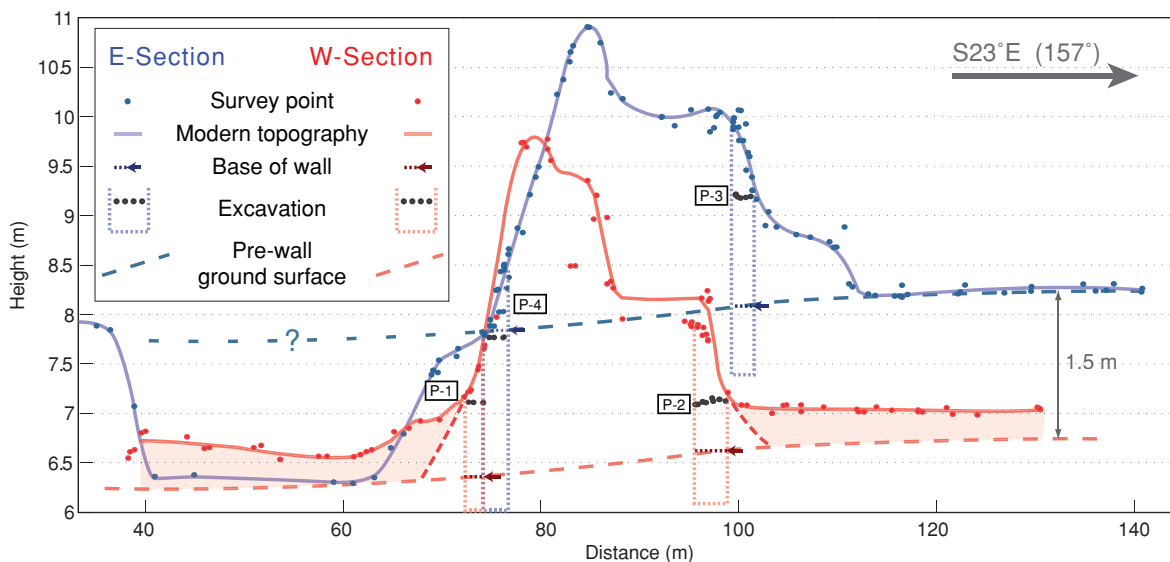


**Figure 3.** Survey profiles across the northern fortress wall. Blue points are east of the fault and red points are west of the fault (that is, the red points are on the viewers side of the fault and the blue points are on the opposite side). All survey points are projected onto a line oriented  $157^\circ$ , perpendicular to the wall. Blue and red lines indicate the modern shape of the fortress wall. P-1 through P-4 indicate the four pits in Figs 2(c) and 4. Dotted polygons show the cross-section of each pit, perpendicular to the wall. Short dashed lines and arrows show the base of the fort wall revealed in the pits. Blue and red dashed lines illustrate the original topography on each side of the fault, prior to the construction of the fortress. The red shadows indicate the thickness of post-fortress sediment on the downthrown (west) of the fault.

also the geometry of the wall. The fault scarp height decreases from  $\sim 1.4$  m at the northern wall to  $\sim 20$  cm 270 m to the south. The change of scarp height is an indication that the vertical component of slip varies along strike, a common observation along strike slip faults (Yeats *et al.* 1997). The northern fortress wall has been obliterated in the vicinity of the fault trace but is still clear on either side. The topographic saddle between the eastern and western section of the fortress wall may be the result of fluvial erosion after tectonic damage.

Estimation of offset on the northern fortress wall is complicated by the fact that the separation of the northern edge of the wall differs markedly from the separation of the southern edge. The width of the wall east of the fault is greater than that west of the fault. This width disparity may result from greater post-offset sedimentation on the downthrown western section of the wall. We tested this hypothesis by studying the stratigraphy in four pits dug through the wall (1–4 in Figs 2c and 3). In each excavation, we identify the contact between the wall and the underlying original sediment (Fig. 4). Each pit exposes a section of manmade fill, consisting of massive yellowish silt to sand with very small amounts of reddish brick and pottery fragments. This fill overlies layers of organic-rich clay to silt and less-organic brown silty sediments. Except for the organic-rich layer, it is not easy to correlate the natural sediments in these four pits. Such spatial variation in floodplain deposits is not uncommon. The organic-rich layer in these pits usually shows a sharp upper and a gradational lower boundary. These characteristics suggest an immature soil that was buried rapidly by construction of the earthen wall.

We found one charcoal fragment in Pit-1, in the floodplain sediment 15 cm below the base of the wall (Fig. 5). Radiocarbon analysis yielded an age of about 4514 BP. However, another radiocarbon age, 32 cm below the base of the wall in Pit-1 ranges from 1210 calendar years (C.E.) to 1390 C.E., with 1210–1300 C.E. being the most likely range (Table 1). Since this younger age should predate the date of fortress construction, the implied date of construction of the fortress wall is during or after the 14th century.

Note that the base of the fortress wall is about 30 cm below the ground surface west of the fault. This indicates a small amount of sediment has accumulated and slightly narrowed the width of the wall. The profile of the upthrown, eastern side does not show an accumulation of post-construction sediment (Fig. 3). Instead, we found evidence for about 1.5 m of erosion north of the wall. Sedimentation to the west of the fault and erosion to the east of the fault require a more careful reconstruction of the offset than a simple matching of the modern topography of the embankment.

To estimate the amount of offset, we first restore the geometry of the fort wall on the downthrown (west) side of the fault by removing the post-construction deposit (Fig. 5). The two pit walls on the downthrown side show the elevation of the ground surface prior to wall construction. We then extend the fort wall profiles to the pre-wall ground. We also restore the pre-wall topography of the northern side of the fort wall on the upthrown (east) side by replacing the eroded post-construction sediment. The estimated edge of the fort wall highly relies on the slope we chose to represent the original wall shape. Here we choose a slope range from  $7.5^\circ$  to  $20^\circ$ , with the maximum slope close to the typical angle of repose for silt ( $19^\circ$ ; Cobb 2009).

Fig. 5 shows the final restored geometries of the fortress wall. The restored fortress wall geometries are similar to each other. Both east and west of the fault, the embankment crest is closer to the northern edge of the embankment than to the southern edge. Also, the height of fort wall east of the fault is similar to its height west of the fault—about 3 m. The widths are also similar: 37 m wide east of the fault and 30.5–35-m-wide west of the fault. The widths of the fort wall 1.5 m above the original ground surface are identical, about 22 m. These similarities support our restoration of the original topography of the embankment near the fault trace.

To estimate the amount of offset recorded by the northern embankment, we select its three clearest piercing points. Its northern base, the southern base, and the crest. Measured perpendicular to the embankment's trend, these three features are separated 4.6–6.9, 5.8 and 8.8–11.7 m across the fault. To determine the equivalent

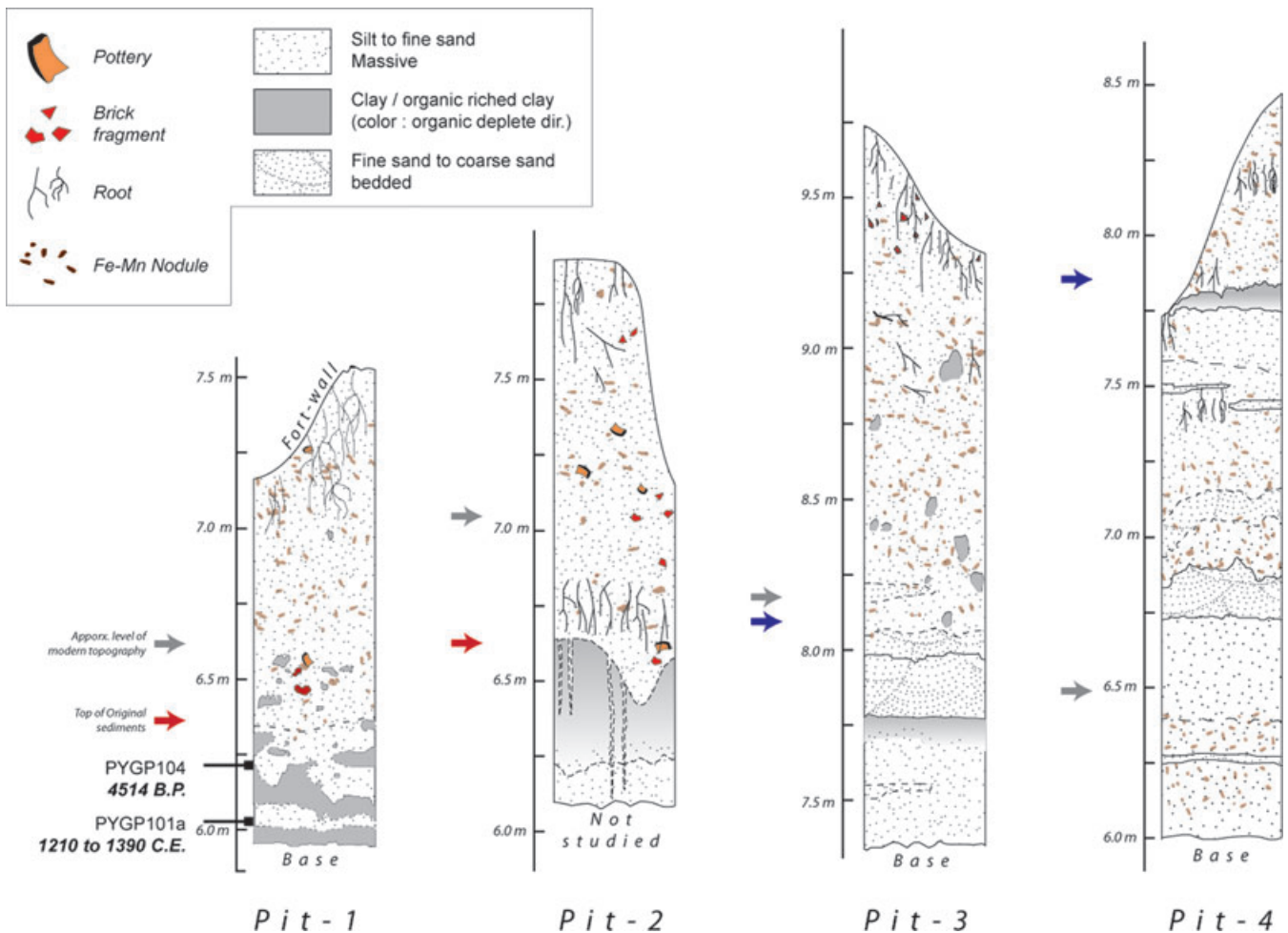


**Figure 4.** Stratigraphic columns of the four pits dug through the base of the fortress wall (Fig. 3c). Blue and red arrows indicate the base of the fortress wall and ground surface prior to construction. Light-grey arrows show the projected elevation of modern topography from inside and outside of the fortress.

three offsets, we must make a trigonometric correction, to measure the offset parallel to the fault trace. This correction is the cosine of the angle between the orientation of the fault ( $180^\circ$ ) and the profiles ( $157^\circ$ ). Both the separations and the derived offsets appear on Fig. 5.

The estimates of separation are less precise for the base of the embankment, because of the uncertainty in extending the topographic profile of the wall downward to the original ground surface. The northern and southern walls display separations of 5–7.5 and 9.5–13 m, respectively (Fig. 5). The matching of the crest gives a more precise estimate of 6.3 m. The separation of the southern base of the fort wall is almost twice as large as the other two measurements. This is most likely the result of agricultural modification. A local farmer claimed that other farmers modified the southern base to create a paddy field about 20 years ago. They dug into the southern slope of the embankment on the upthrown side and used the sediment to create a small but elevated paddy field. As a result, the current southern edge of the embankment is 4–5 m further south than its original position. In light of this history of modification, we discard the 9.3–13 m estimate of separation for the southern flank of the embankment.

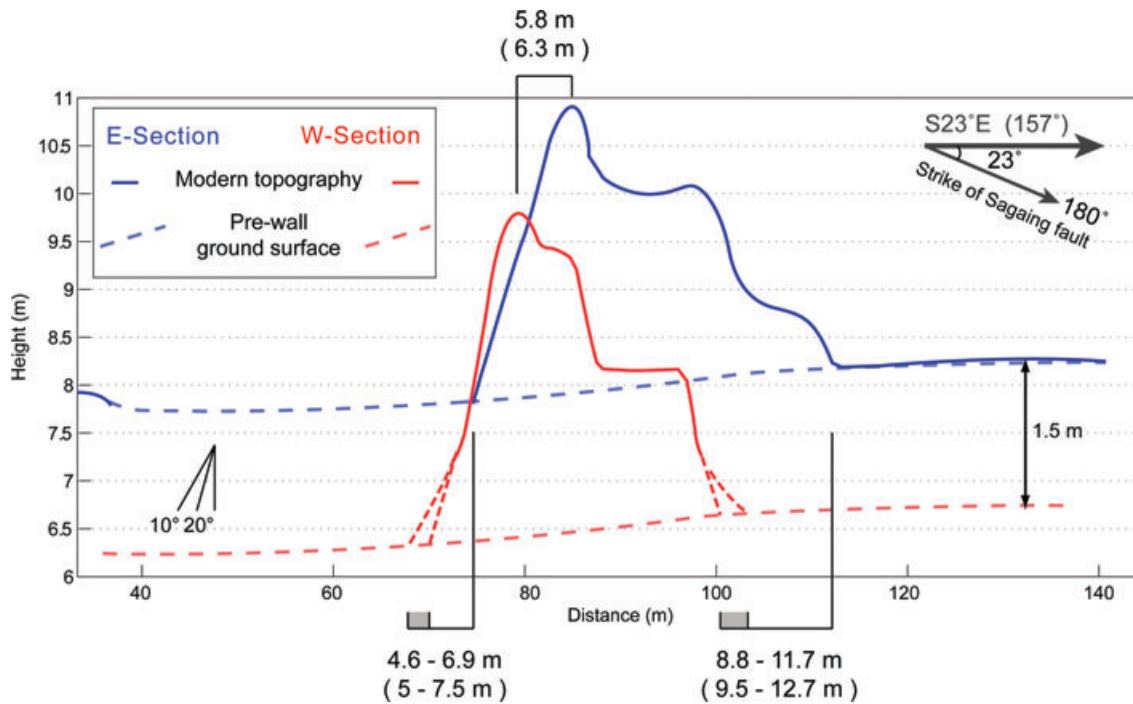
### 3.3 Offset reconstruction

Fig. 6 depicts the history of the embankment at its northern intersection with the fault. First, the perfectly linear embankment

appears on undeformed fluvial plain across the Sagaing fault. Next, oblique slip of the Sagaing fault offsets it. During subsequent rainy seasons, eastward-flowing flood-waters deposit sediment onto the downdropped surface west of the fault. These flood-waters also eroded the faulted wall and surface east of the fault. Repetition of this process not only reduced the height of the fault scarp, but also reduced the apparent horizontal offset on the northern flank of the fort wall and enlarged the apparent horizontal offset on the southern flank of the fort wall.

With this working scenario, we further carry out a simple simulation to estimate the horizontal offset more precisely (Fig. 7). The idea of this simulation is to balance any vertical topographical change after the construction. This simulation also allows us to examine the fault separation derived from the previous section (Section 3.2). We first subtract 1.5 m of elevation from the uplifted surface of the eastern section (Fig. 7b). This step removes the elevation difference due to faulting. We then add back about the same amount of sediments to the eastern section to make up for the sediment surplus and lost due to the post-construction deposition and erosion (Fig. 7c). This step eliminates the influence of differential sedimentation. At the last step, we can offset the eastern profile back to visually match the western profile, and determine the horizontal offset (Figs 7d and e).

The visual matching of the overall fort wall profiles (Figs 7d and e) suggests a separation of 4.8–5.8 m, which corresponds to a fault



**Figure 5.** Fort wall geometry after restoration by removal of post-fortress sedimentation and erosion. The red dashed line shows the inferred geometry of fortress wall west of the fault. The numbers not in parentheses are the horizontal separations perpendicular to the wall at the edges and the crest of the fortress wall. The numbers in parentheses are the fault offset, using a simple cosine correction that takes into account the difference in angle between the orientation of the profile ( $157^\circ$ ) and the strike of the fault ( $180^\circ$ ).

**Table 1.** Analytical results of all of the samples dated in this research.

Radiocarbon age in the Payagyi ancient fortress										
Location	Sample	Lab no.	Stratigraphic unit	$\delta^{13}\text{C}$ (‰)	$^{14}\text{C}$ age (BP)	+/- (BP)	Calendar year ( $2\sigma$ )			Sample type
							From (C.E.)	To (C.E.)	Probability	
Trench (T-1)	PYGP801	AA86448	g-e	-26	940	38	1010	1180	95.4 per cent	Charcoal
	PYGP805	AA87349	e (top)	-28.4	965	36	1010	1160	95.4 per cent	Charcoal
	PYGP806	AA86450	e	-27.3	898	38	1030	1220	95.4 per cent	Charcoal
	PYGP807a	Beta-268175	h-b1	-27.8	980	40	990	1160	95.4 per cent	Charcoal
	PYGP809	AA87347	e	-27.3	882	38	1030	1230	95.4 per cent	Charcoal
	PYGP810	AA87346	e	-28	922	36	1020	1210	95.4 per cent	Charcoal
	PYGP811	AA87348	e (bottom)	-25	2295	80	-750	-100	95.4 per cent	Charcoal
	PYGP814	AA18449	b1-g	-26.2	969	38	990	1160	95.4 per cent	Charcoal
Pit-1	PYGP104	AA86447	Sediment (-15cm)	-23.5	4514	76	-3500	-3450	2.5 per cent	Charcoal
	PYGP101a	Beta-268173	Sediment (-32cm)	-13.9	740	40	1210	1300	92.4 per cent	Organic sediment
							1360	1390	3.0 per cent	

*Note:* The calendar year is converted by Oxcal 3.1, with Intcal'04 Calibration curve.

offset between 5.2 and 6.3 m. This estimation is slightly smaller than the previous estimations made by matching the crest and the base of the fort wall (5–7.5 m). The advantage of this simulation method is that it is not reliant on matching the southern flank, which has been modified by farmers. The only thing that matters is the fort wall geometries on both sides of the fault. This result also confirms our interpretation that the fault separation estimate from the southern base of the fort wall is too large. Thus, the Sagaing fault offset that is recorded by the fortress wall is between 5 and 7.5 m, most probably ~6 m.

#### 4 PALAEOSEISMOLOGIC EXCAVATION IN THE ANCIENT FORTRESS

A trench across the fault ~300 m south of the northern fort wall reveals a partial post-embankment earthquake history. The location of this hand-dug trench is shown in Fig. 2(c). The fault scarp across the paddy fields there is 10–20 cm high. Contrasts in sediment colour and grain size are faint in this trench. Most sediment is silt and clay, which we interpret as overbank deposits. These sediments are also strongly bioturbated, so few sedimentary contacts are apparent in

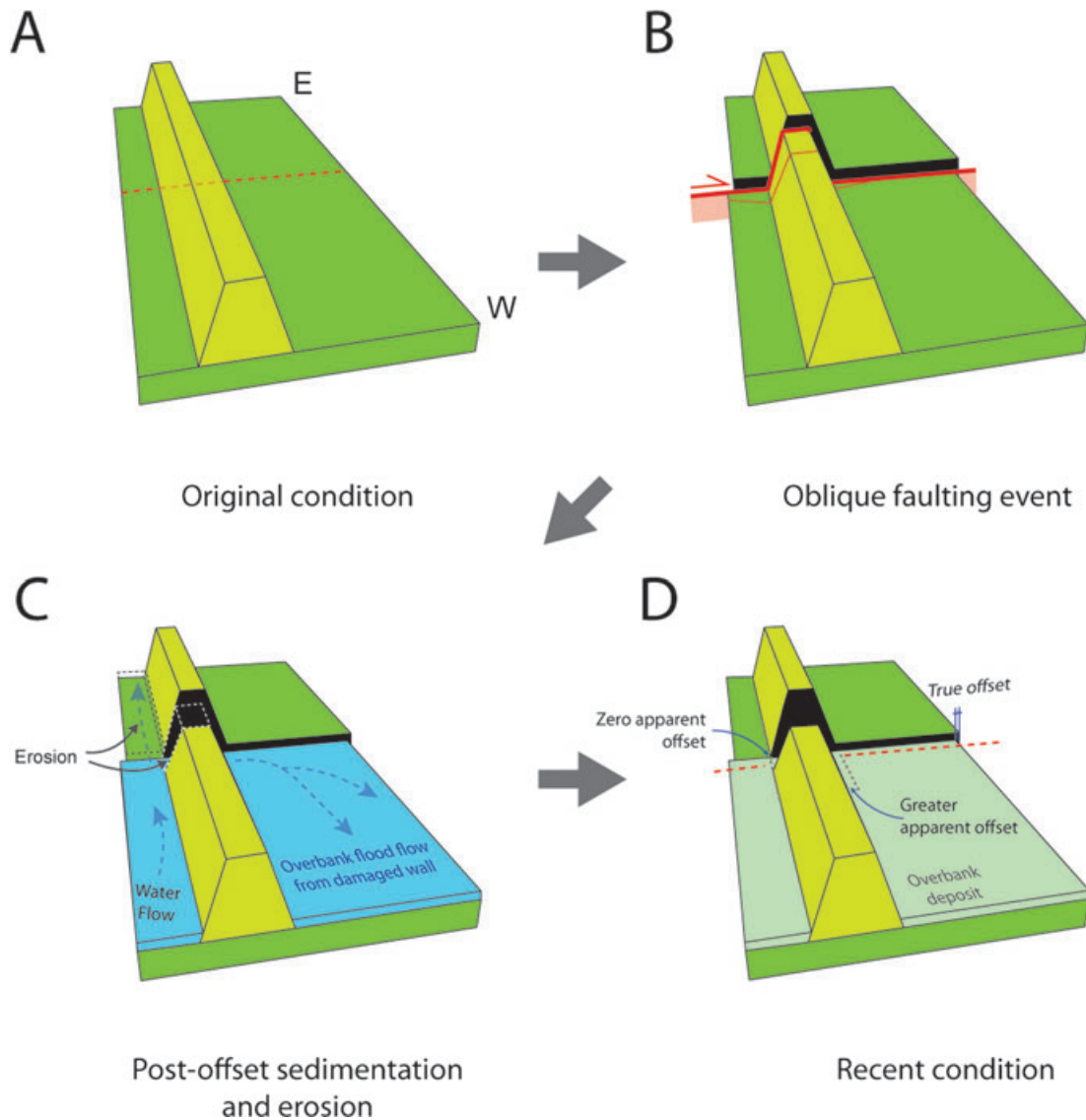


**Figure 6.** This schematic model shows the relationship of the Sagaing fault rupture to the sedimentation on the downthrown side near the northern fortress wall. See detail in Section 3.3.

either wall of the trench. These sediments are therefore far from optimal for providing a detailed palaeoseismologic history.

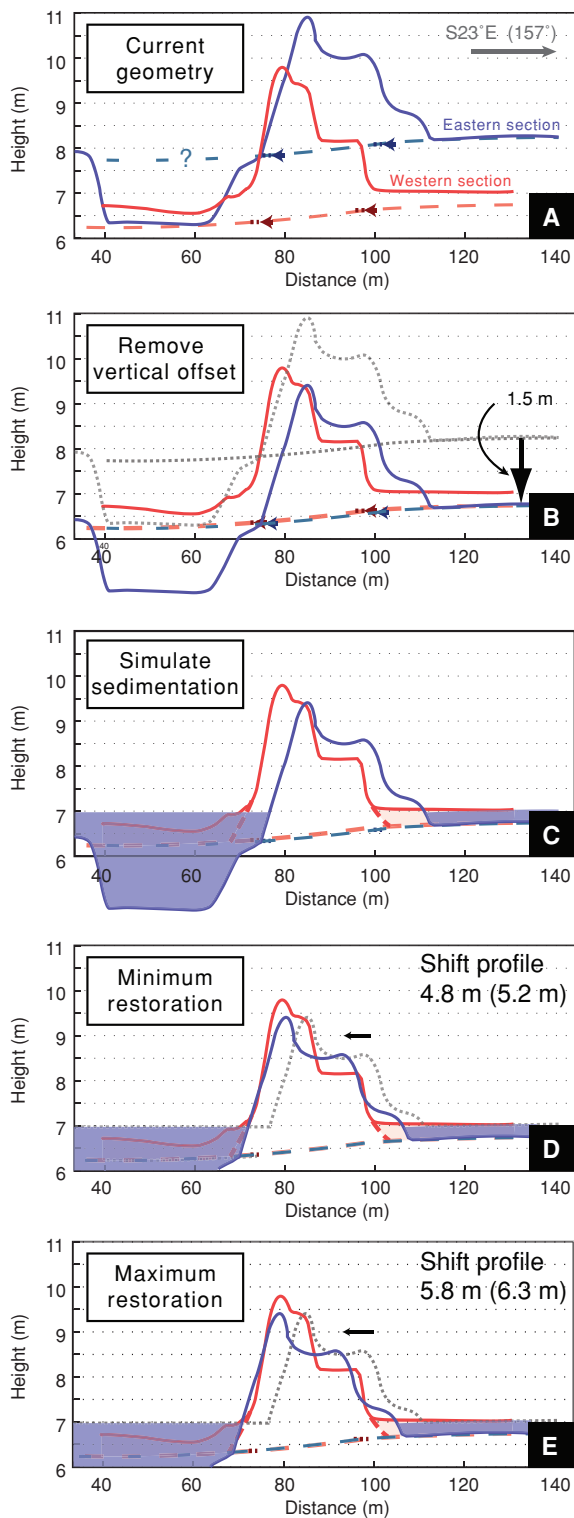
#### 4.1 Sedimentary units in the trench

Fig. 8 is a map of the southern wall of the trench. This map shows six main sedimentary units: a topmost grey to orange mottled massive silt (a), a massive medium grey mottled clayey silt deposit (b), a dark organic-rich clay (h), a med-grey pedogenic clayey silt that is rich in dark, hard nodules (b1), a clayey silt layer that is rich in brick fragments (g) and a massive silty clay layer (e). All of these units exhibit extensive bioturbation, predominantly by crabs, which can penetrate from the ground surface to depths as great as 2–3 m. Sediment fills some of the crab burrows; other burrows are hollow but have 5- to 10-mm-thick clay films lining their walls. We have mapped the burrows where they are clearly visible, but other burrows may have gone unrecognized.

Overlying all other units exposed in this trench is a massive cultivated silty layer. This deposit, labelled as layer (a), consists of

a 20–40 cm thick, grey to orange mottled massive silt. The topmost part of layer (a) is a 2-cm-thick light-grey loose silt, uniformly distributed on the paddy field and the paddy field boundary. This thin layer of silt is the most recent suspension deposit from flooding in the rainy season. Layer (a) is thicker on the northeastern side of the trench than it is on the southwestern side of the trench. It is because the northeastern side of the trench cuts across the paddy field berm, so the surface elevation of the northeastern side reflects the height of paddy field boundary, not the height of a fault scarp.

Unit (b) underlies the cultivated layer (a). This dry massive clayey silt layer is harder than overlying unit (a) and is distinctly darker. Unit (b) is about 40–60 cm thick and is composed of massive medium grey mottled clayey silt with very rare submillimetres to millimetre brick fragments. These fragments usually appear as dark-red to orange specks. The thickness of unit (b) increases gradually towards the northeast. Although the contact between units (a) and (b) is gradational over ~5 cm, it is clear that the contact is ~10 cm higher on the northeastern side of the trench than on the southwestern side. This contact may reflect the topography of the ground surface before it was modified to form the modern paddy field.



**Figure 7.** A sequential restoration of the fortress wall offset. (A) The current relationship of the eastern (blue) and western (red) sections of the fortress walls, as viewed along the axis of the wall. (B) Relationship after removal of the vertical offset from the eastern (distant) profile, as judged by the difference in elevation between the original, pre-fortress land surfaces. For reference, the grey-dashed line shows the original location of the eastern profile. (C) Addition of sediment on top of the eastern section, to equal the amount of sediment that accumulated on the downthrown, western profile. (D) Relationship after restoring the minimum right-lateral offset, 5.2 m. (E) Relationship after restoring the maximum right-lateral offset, 6.3 m.

Unit (h) underlies unit (b) and is the most notable unit in the trench. This 8-cm-thick organic unit (h) is dark-grey organic clay. The unit has a sharp upper contact with overlying unit (b) and a gradational lower boundary marked by a colour change. This morphology suggests it is a topsoil layer that was later buried by deposit (b) and (a). Its upper contact is coincident with the uppermost occurrence of hard, black Fe–Mn-rich soil nodules.

Under the thin palaeosol is the med-grey mottled massive clayey silt. We mark this layer unit (b1), because its composition is similar to that of unit (b). Hard, black Fe–Mn soil nodules are common within this unit but do not exist in unit (b). These subangular to rounded hard nodules are usually smaller than 7 mm in diameter.

This unit also contains a very small percent of brick fragments that range in size from about 3 to 7 mm. These fragments increase upward in concentration, to about 20 per cent at the top of the unit. This characteristic of the unit is distinct throughout the trench exposure, so we separate the brick-rich band as another mappable unit, (g). The size of these subangular brick fragments ranges from subcentimetre to more than 5 cm. In none of these fragments is the original shape of the bricks preserved. Many fragments of charcoal co-exist with these fragments. The structure of the charcoal indicates it is the product of the burning of wood. These 5-mm to 1-cm-size pieces are commonly subrounded to rounded, which is an indication that they have been transported by water from their source, either a campfire or a burning timber.

Radiocarbon ages of charcoal from close to the upper and lower contacts of unit (g) (samples P814 and P801 in Table 1) are 990–1180 C.E. (Table 1).

The lowest unit exposed in the trench unit (e) is undifferentiated massive silty clay. This deposit consists of light grey to orange mottled silty clay, with thin lenses of light orange silty sand near the base of the trench. The hard, dark Fe–Mn nodules are also abundant in this deposit. Their concentration in this unit is similar to that in the overlying two layers. Rare small fragments of brick exist in the upper 25 cm of this deposit. We recovered several pieces of charcoal in this unit. They were angular to subangular rectangular forms, with woody cellular structures preserved. Radiocarbon analyses of charcoal from the upper part of unit (e) (samples P807, P805, P806 and P809 in Table 1) yield ages similar to those of samples in unit (g), 990–1230 C.E. A single radiocarbon date from several charcoal clasts (P811) at the base of the trench, yielded much older age (750–100 B.C.E.).

The fact that the radiocarbon ages of seven samples of charcoal from different strata within the trench are similar (990–1230 C.E.) suggests two possible interpretations. Either all these units below palaeosol (h) formed in two hundred years or less, by very rapid deposition of very fine grain material, or their charcoal originated from material with that range in ages. In the former case, the strata would be well dated by the charcoal ages. In the latter case, the dates of sedimentation are the same as or younger than the charcoal ages.

The fact that all seven samples yielded older ages than the age of organic material (PYG0101a in Table 1) under the fortress wall is important in interpreting the date of construction of the embankment. If these dates represent the age of the strata, brick-rich layer (g) is at least 200 years older than the fortress, and we might expect to observe another cultural layer above unit (g), related to the fortress construction. However, no such cultural horizon exists above the brick layer (g). Thus, we suggest these fragments originated upstream as burned construction timbers. Traditional Burmese buildings were constructed of timber and brick. This style of construction still existed in the 16th century royal palace in Bago. If the embankment served as military defence structure within the

same period, we would expect to find the remains of similar construction materials within the confines of the ancient walls. The mixture of brick and charcoal fragments in the trench strata lend support to this hypothesis. Therefore, it is reasonable to interpret these fragments of charcoal as the cooled embers of construction timbers that were burned during or after the destruction of the fortress and were later transported and buried at the trench site. Thus, we suggest that the radiocarbon ages of these fragments are greater than the depositional age of these sediments.

#### 4.2 Fault traces on the southern trench wall

We found two plausible faults in the southern wall of the trench, which extend above the brick-rich unit (g) (I and II in Fig. 8). Because all of the faulted strata are extensively burrowed and have lost their fine structure, we cannot recover many details of the faulting, including any minor faults in the wall of the trench. Thus, our interpretation of faulting relies principally on changes in elevation of stratal contacts.

Fault I is the younger of the two. Units (g) and (h) have an abrupt 8 cm vertical discontinuity across Fault I. Bioturbation obscures the upward termination of the fault in unit (b). There is no direct evidence that Fault I breaks the upper contact of unit (b). However, that contact does have an elevation change of several cm across the upward projection the fault. Moreover, the thickness of unit (b) is not greater on the downthrown side, which suggests it did not form after faulting.

Fault II is the older of the two faults. It disrupts the brick layer (g) but does not appear to affect overlying palaeosol (h). Its sense of vertical separation is towards the east, opposite the direction of the fault scarp visible in the topography. The youngest rupture of Fault II clearly post-dates deposition of brick-rich layer g. However, it must antedate the formation of palaeosol h, since Fault II does not disrupt the palaeosol.

Two other features may also indicate a rupture between the formation of units g and h. The funnel shape of the lower contact of layer (g) east of the fault could reflect filling of a ground fissure

that formed before the formation of palaeosol (h). The U-shape downward protrusion of unit b1 into unit e might also indicate a fissure that formed between deposition of units g and h. If these are, indeed, the result of faulting between deposition of units g and h, the simplest hypothesis is that they formed at the same time as the scarp of Fault II.

Fault I may have last moved during either the 1930 earthquake or during an earlier rupture, or both. It is conceivable that the small vertical separation at the base (and possibly the top) of unit b reflects minor slip near the northern terminus of the 1930 rupture. If the top of unit b is not disrupted, it is also possible that Fault I broke during a rupture earlier than 1930. There are no local farmers old enough to attest to effects associated with the 1930 earthquake and we found no datable materials in unit b to constrain the date of the rupture.

Fault II broke after the formation of brick layer (g) but before the formation of palaeosol h. Assigning a date to this rupture depends upon one's interpretation of the age of these two units. We have hypothesized that radiocarbon dates from charcoal in that layer and layer b1 are older than the units themselves, having come from campfires or burnt timbers upstream. We also hypothesize that the brick-rich layer g is associated with the destruction of the fortress. If these hypotheses are correct, then Fault II ruptured either during or after destruction of the ancient fortress. In summary, these two fault ruptures suggest two or more faulting events, possibly including the 1930 earthquake, after the destruction of the fortress.

## 5 DISCUSSION

### 5.1 The age of ancient fortress

The radiocarbon dates from charcoal within and beneath brick-rich unit (g) provide an oldest plausible range of dates for construction of the fortress—990–1230 C.E. Celadon potteries that we found in nearby paddy fields were produced in the 15th or 16th century (Bob Hudson, field conversation, 2008). Although these fragments were sitting on the modern, cultivated surface, their presence implies

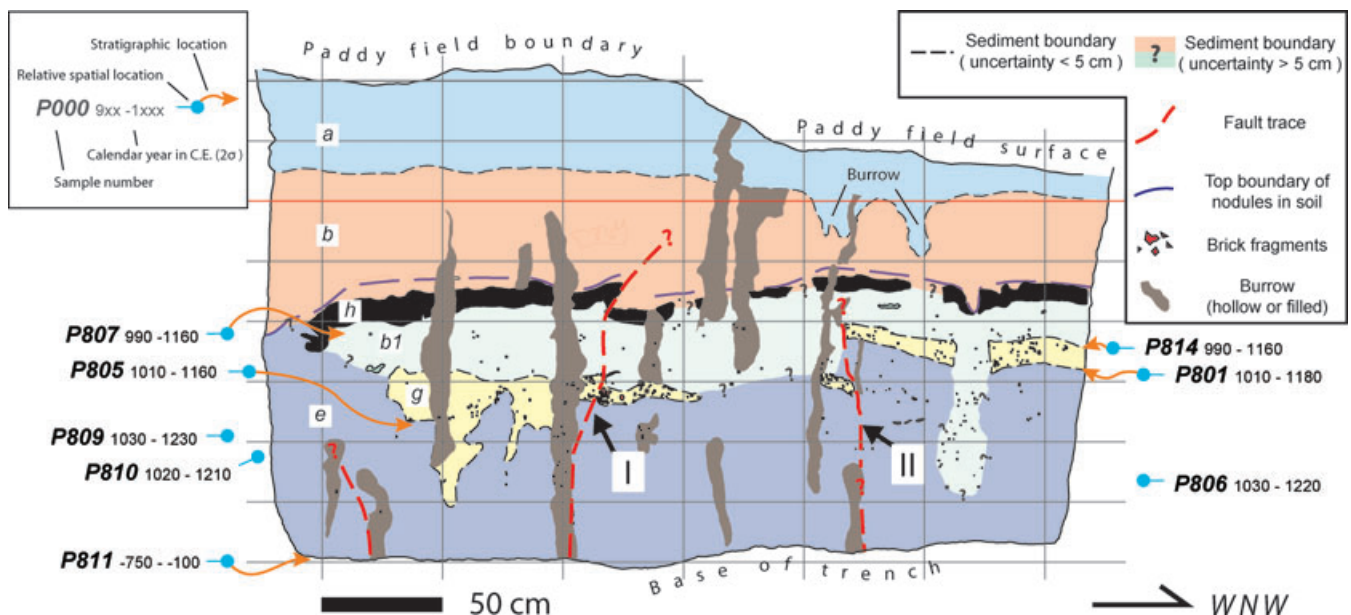


**Figure 8.** Map of the southern wall of Trench 1. Grid is 50 cm × 25 cm. I and II mark two possible fault traces, which appear to extend upward to two discrete horizons. Thus, they may reflect the occurrence of two distinct events, between the time of the abandonment of the ancient fortress and the 1930 Pegu earthquake. Blue dots show the stratigraphic location of radiocarbon samples. The  $2\sigma$  range of the ages is in calendar years (C.E.).

human activity at the site during the 15th or 16th century. The occurrence of only a single cultural horizon within the trench strata implies that the fortress operated only for a short period.

The youngest plausible date of construction of the Payagyi ancient fortress is 1634 C.E., the year that Bago ceased being the capital of the country. Its loss of importance at that time deprived the kingdom of any reason to build such a well-designed defensive structure nearby. Although Bago once again became the capital of the Mon people from 1740 to 1757 C.E. (Ooi 2004), we found no archaeological evidence that the fortress had been used during this period.

The historical, radiometric and stratigraphic data thus imply that the ancient fortress was most likely built between 990 and 1634 C.E. Moreover, history tells us that only in the latter half of that period, between 1369 and 1634 C.E., was Bago the regional political centre of this area (Lieberman 1980; Ooi 2004). It was the capital of the Mon kingdom from 1369 to 1539 C.E. and was the official capital of Burma from 1539 to 1599 C.E. and 1613 to 1634 C.E.

If this rectangular earthen structure 16 km north of Bago was built to protect the city, the timing of its construction and operation would thus have to fall between the mid-14th century and early 17th century. Furthermore, the rectangular earthen structure shares the same architecture form with the wall of Pegu city (also rectangular), which was built when Pegu was the official capital of the country between 1539 and 1599 C.E. (Fedrici 2004), so we believe the construction and use of this earthen structure would most likely also occur during this period, before the city of Pegu was ruined by the war.

This interpretation is not in conflict with the radiocarbon age of organic material under the fortress (PYG0101a), which constrains construction of the embankment to after a date in the range of 1220–1300 C.E. Also, it is not in conflict with the history recounted

in the introduction, in which we suggest that the structure could have been built in 1574 C.E. for temporary royal use.

## 5.2 Late Holocene slip rate along the southern Sagaing fault

We can now use the constraints on the age of the embankment to constrain the slip rate of the Sagaing fault over the past few hundred years. The 5–7.5 m offset of the northern fortress wall has accrued since a date in the range of 1369 and 1634 C.E. Dividing the range of offsets by the range in dates yields a range in slip rate of 8–20 mm yr<sup>-1</sup>. If we assume a tighter range in construction dates, 1539–1599 C.E., when the city of Pegu was the official capital of the country, the range of fault slip rate narrows to 11–18 mm yr<sup>-1</sup>. We favour a slip rate of 14 mm yr<sup>-1</sup>, calculated by dividing the best estimate of offset, 6 m, by the age of the embankment, assuming it was built for temporary royal usage in 1574 C.E.

This fault slip rate is, of course, an aliased estimate, in that we have not considered where in its seismic cycle the fault was at the time of embankment construction or is now. Our slip rate is comparable to two slip-rate estimates 500–550 km further north along the fault (Bertrand *et al.* 1998; Vigny *et al.* 2003). The similarity of our estimate to theirs implies that the slip rate does not vary appreciably from 23°N to lower Myanmar (17.5°N). If the slip rate along the Sagaing fault varies significantly at different latitudes, we should have observed other subsidiary structures to accommodate the differential slip rates along the Sagaing fault. The lack of such structures along the Sagaing fault is consistent with our interpretation of no significant rate difference between the central and southern Sagaing fault.

The similarity also implies that the averaged slip rate has been time-invariant for the past quarter million years (Fig. 9). Our

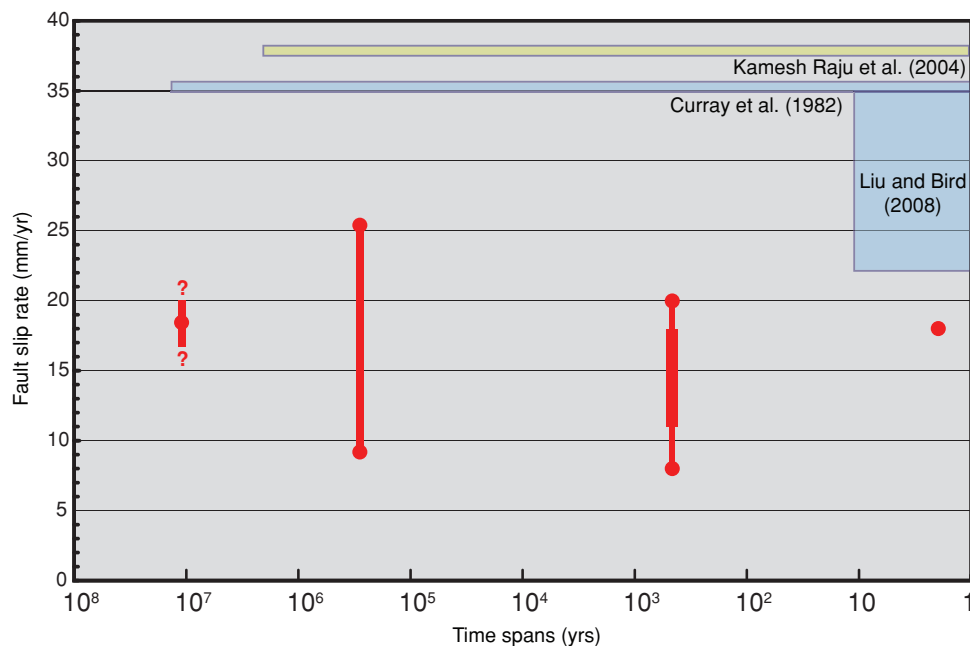


**Figure 9.** Slip-rate estimations along the Sagaing fault averaged over different time spans. Rates based upon models (green and blue) are greater than those based upon field observations (red). Red dots are the maxima and minima of different estimated slip rates, based on features offset by the central and southern Sagaing fault or on geodetic measurements made in 1998 and 2000. From left to right, the data sources are Myint Thein *et al.* (1991), Bertrand *et al.* (1998), this study and Vigny *et al.* (2003). For the fault slip rate from this study, the thick red line indicates the range of fault slip rate based upon construction of the ancient fortress between 1539 and 1599 C.E. Blue coloured boxes show the slip rate predictions from a block-motion model and a general transform-fault model. Green box is the spreading rate at the Central Andaman sea spreading centre (38 mm yr<sup>-1</sup>, Kamesh Paju *et al.* 2004). Slip rates based upon the block model are much greater than the slip rate of the Sagaing fault.

slip-rate estimation is not only similar to the current rate from the short-term geodetic observation across the central Sagaing fault (Vigny *et al.* 2003), but is also similar to the long-term averaged slip rate estimated by Bertrand *et al.* (1998) at the offset Singu basalt flow, in central Myanmar. Myint Thein *et al.* (1991) also suggest a similar averaged rate,  $18.5 \text{ mm yr}^{-1}$ , based upon a metamorphic belt offset across the central Sagaing fault. Although they did not have a solid constraint on the timing of fault initiation, the similarity of their result may imply little or no variability over an even longer interval—10 Myr.

All four of these estimates are slower than those inferred from broader-scale models (Curray *et al.* 1982; Meade 2007; Liu & Bird 2008). Meade's microplate model does not include an active convergent boundary (megathrust in Fig. 1) between the Indian and Burma Plate. Therefore the difference between his rate prediction and these slip-rate estimations could result from the slip partitioning between the Sagaing fault and the megathrust or from deformation within the Burma Plate. On the other hand, Liu and Bird's kinematic plate model does consider a separate Burma Plate. However, their model also predicts a higher Sagaing fault slip rate than other geological and geodetic estimations. Again, this disparity suggests that either there is significant deformation within the Burma Plate or that the initial fault-slip parameters in their model are inappropriate.

Another issue is the difference between the spreading rate in the Andaman Sea Basin ( $38 \text{ mm yr}^{-1}$ ) and the observed slip rate on the Sagaing Fault (Fig. 9). We can explain this difference again by internal deformation of the Burma Plate, and/or by plate rotation. Gahalaut & Gahalaut (2007) demonstrate how plate rotation and plate geometry affects the fault slip rate in this area. Their model shows a nearly constant  $16\text{--}17 \text{ mm yr}^{-1}$  fault slip rate along the Sagaing fault, which agrees with the rates derived from fault-crossing studies. However, their parameters predict a much lower spreading rate ( $21 \text{ mm yr}^{-1}$ ) in the central Andaman Sea spreading centre than the rate that previous study suggests ( $38 \text{ mm yr}^{-1}$ , Kamesh Raju *et al.* 2004). Despite this disparity, their result still points out that part of the slip rate disparity between the spreading centre and the transform fault may result from the relative plate rotation between Burma and Sunda plates. These discrepancies in rates show that more attention needs to be paid to the possibilities of internal deformation and the relative motion of the Burma Plate.

### 5.3 Seismic potential and behaviour of the southern Sagaing fault

In this last section of the paper, we will discuss the seismic potential of the southern Sagaing fault. We will also construct speculative fault slip scenarios along the southern Sagaing fault for the past 500 years. We use the meager evidence from the Payagyi fortress trench, measurements of fault displacement associated with the 1930 May earthquake, intensities from the 1930 December earthquake and the history of damaging earthquakes from nearby cities to construct our fault-slip scenarios. This exercise helps us evaluate the future seismic potential of the southern Sagaing fault.

The pattern of surface rupture associated with the Pegu earthquake in 1930 raises an interesting issue concerning the fault-slip behaviour of the southern Sagaing fault. Since the slip distribution curve has a bell-shaped pattern and the active fault trace continues both to the north and south of the rupture (Fig. 1c), the 1930 rupture cannot be representative of all ruptures along that portion of the fault. Along at least a 50-km-long section of fault between  $17.5^\circ\text{N}$  and  $18^\circ\text{N}$ , shaking intensity was low during the last two

significant earthquakes in the region, the Pegu ( $M_s$  7.2) and Pyu ( $M_s$  7.3) earthquakes in 1930. This section of the fault is either locked or creeping. In either case, it did not fail during the 1930 sequence. Not only does this section lack moderate seismicity in the global seismic catalogue over the past three decades, but local villagers we interviewed also claimed that they had only experienced two to three earthquakes in their life time. These observations suggest that this section is, indeed, locked. The 50-km length of this section implies that it is capable of generating an earthquake of  $M$  7+ (Wells & Coppersmith 1994). Judging from the fact that this section did not fail during the 1930 sequence, it is a reasonable candidate for the next seismic rupture of the southern Sagaing fault.

Although we lack palaeoseismological and geodetic data along this fault section that would aid in forecasting its long-term seismic potential, we may still provide a reasonable speculation about its seismic behaviour by constructing fault slip scenarios that match our observations along the southern Sagaing fault.

Here we favour a variant of the uniform fault-slip model to explain the slip history of the southern Sagaing fault over the past 500 years. Tsutsumi & Sato (2009) and this study show that the surface displacements near  $17^\circ\text{N}$  are close to 3, 6, 9 and 13 m (Fig. 1c). Although these field observations are sparse, mostly because small tectonic landforms have been easily destroyed over the centuries by flooding and agricultural activities on the active fluvial plain, they still seem to indicate that fault slip along the central portion of the 1930-rupture is close to 3 m. This bell-shaped pattern of these smallest offsets supports a uniform slip model for fault-slip behaviour along the southern Sagaing fault.

We propose two fault-slip scenarios for the southern Sagaing fault. These scenarios cover the straight section of the fault trace from  $16.5^\circ\text{N}$  to  $18^\circ\text{N}$ . For the purpose of constructing these speculative scenarios, we assume that the bend in the Sagaing fault at  $18^\circ\text{N}$ , which has an unusually high degree of background seismicity, is a low-coupled patch that presents a natural northern limit to large seismic ruptures (Fig. 1b).

Next, we use field measurements of small tectonic offsets, our palaeoseismological results at the fortress, historical earthquake accounts and seismic records from the cities of Bago and Yangon to constrain the earthquake rupture history of the past five centuries. The dates of historical earthquakes after 1564 C.E. come from several different sources (Milne 1911; Chhibber 1934; Thawbita 1976; Saw Htwe Zaw 2006; Win Swe 2006). To identify only those events that are likely to have produced large surface offsets, we use only the dates of earthquakes that appear in more than one account (Table 2). We attempt to discriminate further the smaller from the larger events by using other available information. For example, the 1917 earthquake appears in several local catalogues but not in any instrumental catalogues. Moreover, stories we collected from villagers also suggest shaking in 1917 was weaker than in 1930, both north and south of Bago (Table S1). Therefore, we interpret the 1917 event to be moderate in size, and discount the possibility of large surficial fault slip on the Sagaing fault.

The age of the Payagyi ancient fortress and our palaeoseismology evidence for the number of fault ruptures since its construction also help us constrain the earthquake history. The fortress was most likely built in 1574 C.E. and has been offset by at least two earthquakes (three if one allows the possibility that a small amount of slip occurred there during the 1930 earthquake). Furthermore, our best estimate of total offset of the fortress wall is 6 m, which constrains the cumulative slip since 1574 C.E. there.

All of these constraints on earthquake rupture history have gone into the construction of Scenario-1 (Fig. 10a), which also

**Table 2.** Earthquake and damage record from different sources near Bago from 875 C.E. to 1930 May C.E.

Chhibber (1934) (Rangoon & Bago)	Thawbita (1976) (Rangoon & Bago)	Win Swe (2006) (Bago)	Milne (1911) (Rangoon)	Saw Htwe Zaw (2006) (Rangoon)
		<b>1564</b>		<b>1564</b>
		1570		
		1582	No record at India before 1618 C.E.	
	1588			1608
	1590			1620
No record before 1762 C.E.		<b>1644</b>		<b>1644</b>
				1649
				1652
				1661
				1664
				1679
	Jun-4-1757			
	<b>Jun-12-1768 (Rangoon)</b>	<b>1768</b>		<b>1768</b>
		1830		
1864 (Rangoon)				
1884 (Rangoon)		<b>Oct-8-1888</b>	<b>Oct-9-1888</b>	<b>1888</b>
			Dec-13-1894	
		Mar-6-1913		
<b>1917</b>	<b>Jul-5-1917</b>	<b>Jul-5-1917</b>		
			Catalog ends in 1900 C.E.	1919
1927 (Rangoon)	1927 (Rangoon)			
<b>1930</b>	<b>May-5-1930</b>	<b>May-5-1930</b>		<b>1930</b>

assumes a classical uniform-slip behaviour for the fault (Schwartz & Coppersmith 1984). That is, the pattern of slip is similar from event to event. In this scenario the last event north of Bago occurred in 1888 C.E., with 2.5 m of slip through the ancient fortress. The average earthquake recurrence interval for the section of the fault north of the 1930 surface rupture is 140–180 yr, which we calculate by dividing the fault slip rate of 14–18 mm yr<sup>-1</sup> into 2.5 m of slip per event. Likewise, the average frequency of 1930-type events ( $M$  7.3) is 250–320 yr. Together, these two segments produce a cumulative recurrence of strong earthquakes in the region of Bago ranging between 90 and 115 yr.

An alternative construction that also is faithful to the scant historical, palaeoseismological and slip data is Scenario 2 (Fig. 10b), which uses the form of the uniform slip model proposed for another strike-slip fault, the Imperial Fault (Sieh 1996). In contrast to Scenario 1, slip in repeated events along the 1930 section is characteristically less than along the section farther north. In this scenario, the last major event to break the ancient fortress wall occurred in 1768 C.E., and 6 m of slip occurred farther north. The frequency of strong earthquakes in the Bago region ranges from 167 to 215 yr. In this case, the magnitudes of earthquakes in the Bago region vary from  $M$  7.3 to  $M$  7.5. The largest earthquakes are less frequent.  $M$  7.5 earthquakes occur every 333–430 yr, with stronger shaking at Bago than that during the 1930 event.

Our two uniform-slip scenarios are intended merely to stimulate further discussion and work aimed at understanding the past history and future potential of this important section of the Sagaing fault.

## 6 CONCLUSION

We have measured ~6 m of dextral offset of an ancient fortress wall across the southern Sagaing fault in Myanmar. Historical evidence and radiocarbon dating of relevant cultural and natural strata

imply a most-likely age for the fortress wall of 1574 C.E. Excavations reveal that strata that are younger than construction of the fortress have been offset at least twice by the Sagaing fault. Isoseismals of the historical 1930 earthquake imply that the rupture that caused this  $M$  7.2 earthquake was predominantly south of the fortress and that rupture at the site must have been less than about a metre. This leaves 5–6 m for earlier events subsequent to the late 16th century.

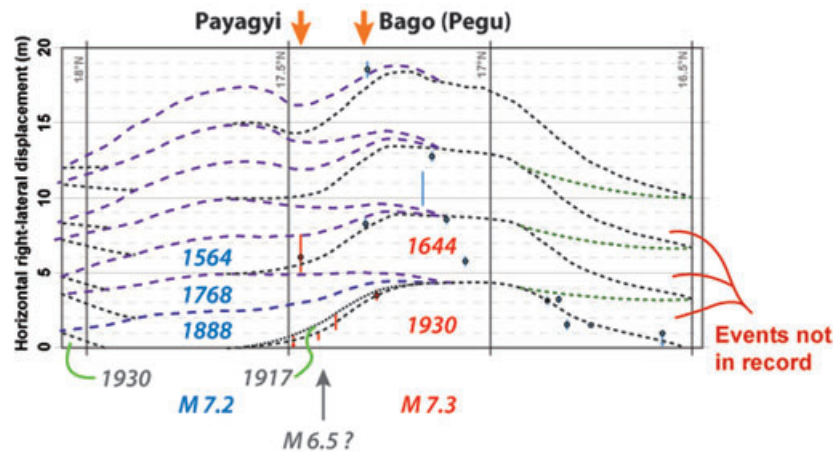
We have constructed plausible uniform-slip models of the earthquake history of this section of the southern Sagaing fault, using the scant available palaeoseismic and historical data. They suggest the existence of two distinct segments of the fault, which together produce return times for destructive earthquakes in the region ranging between about one and two centuries.

The 11–18 mm yr<sup>-1</sup> slip rate that we calculate from the offset fortress wall is significantly slower than the 38 mm yr<sup>-1</sup> rate determined from the spreading history of the Andaman Sea. This discrepancy must be explained either by clockwise rotation of the Burma plate or one or more currently unrecognized structures running northward from the spreading centres into Burma.

## ACKNOWLEDGMENTS

We benefited greatly from discussions with Win Swe, Bob Hudson, J. Bruce H. Shyu and their colleagues. The comments and suggestions of Christophe Vigny and another reviewer also helped us improve this manuscript. We also appreciate the generous support of the Immediate Past President of the Myanmar Engineering Society (MES), Mr. Than Myint, and help from the Myanmar Geosciences Society (MGS), the Department of Meteorology and Hydrology (DMH), the Department of Natural Museum, Library and Archaeology of the Ministry of Culture in Myanmar and Thingazar Travels & Tours Company. This research was supported initially by the

## (a) Scenario -1



## (b) Scenario -2

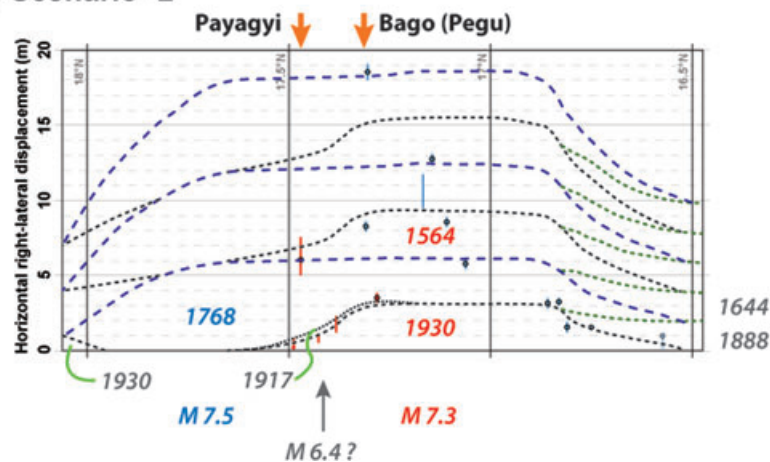


**Figure 10.** Two fault-slip scenarios for the southern Sagaing fault. (a) A classic uniform-slip model. (b) Imperial-fault slip model. Field measurements (blue and red dots and vertical bars) are the same as in Fig. 1c. Coloured dashed lines denote different types of the fault rupture. Red and blue numbers suggest dates for each rupture, based upon the dates of earthquakes known from historical records.

Caltech Tectonics Observatory and later by the Earth Observatory of Singapore (EOS), Nanyang Technological University, Singapore. This is Caltech Tectonics Observatory contribution 140 and Earth Observatory of Singapore contribution 12.

## REFERENCES

- Bird, P., 2003. An updated digital model of plate boundaries, *Geochem. Geophys. Geosyst.*, **4**(3), 1027, doi:10.1029/2001GC000252.
- Berglar, K., Gaedicke, C., Franke, D., Ladage, S., Klingelhoefer, F. & Djajadihardja, Y.S., 2010. Structural evolution and strike-slip tectonics off north-western Sumatra, *Tectonophysics*, **480**(1–4), 119–132, doi:10.1016/j.tecto.2009.10.003.
- Bertrand, G., Rangin, C., Maury, R.C., Htun, H.M., Bellon, H. & Guillaud, J.P., 1998. The Singu basalts (Myanmar): new constraints for the amount of recent offset on the Sagaing Fault, *C. R. Acad. Sci., Ser. IIA, Earth planet. Sci.*, **327**, 479–484.
- Brown, C.J. & Leicester, P., 1933. The Pyu earthquake of 3rd and 4th December, 1930, and subsequent Burma earthquakes up to January, 1932, *Mem. Geol. Surv. India*, **62**, 1–140.
- Brown, C.J., Leicester, P. & Chhibber, H.L., 1931. A preliminary note on the Pegu earthquake of May 5th, 1930, *Rec. Geol. Surv. India*, **LXV**, 221–284.
- Chlieh, M. *et al.*, 2007. Coseismic Slip and Afterslip of the Great (Mw 9.15) Sumatra-Andaman Earthquake of 2004, *Bull. seism. Soc. Am.*, **97**(1A), S152–S173, doi:10.1785/0120050631.
- Cobb, F., 2009. *Structural Engineer's Pocket Book*, 2nd edn, Butterworth Heinemann, Oxford, ISBN-13: 978-0-7506-8686-0, p. 102.
- Curry, J.R., 2005. Tectonics and history of the Andaman Sea region, *J. Asian Earth Sci.*, **25**(1), 187–232.
- Curry, J.R., Moore, D.G., Lawver, L.A., Emmel, F.J., Raitt, R.W., Henry, M. & Kieckhefer, R., 1979. Tectonics of the Andaman Sea and Burma, *Am. Assoc. Petrol. Geol. Mem.*, **29**, 189–198.
- Curry, J.R., Emmel, F.J., Morre, D.G. & Raitt, R.W. 1982. Structure, tectonics, and geological history of the northeastern Indian Ocean, in: *Ocean Basins and Margins*, Vol. 6: The Indian Ocean, pp. 399–450, eds Nairn, A.E.M. & Stehli, F.G., Plenum, New York, NY.
- Chhibber, H.L., 1934. *The Geology of Burma*, pp. 47–70, McMillan and Co. Ltd, London.
- Fedrici, C., 2004. Account of Pegu, Original English edition 1588; reproduced in *SOAS Bul. Burma Res.*, **2**(2), 130–159.
- Fitch, T.J., 1972. Plate convergence transcurrent faults and internal deformation adjacent to South-East Asia and western Pacific, *J. geophys. Res.*, **77**, 4432–4460.
- Gahalaut, V.K. & Gahalaut, K., 2007. Burma plate motion, *J. geophys. Res.*, **112**, B10402, doi:10.1029/2007JB004928.

- Genrich, J.F., Bock, Y., McCaffrey, R., Prawirodirdjo, L., Stevens, C.W., Puntodewo, S.S.O., Subarya, C. & Wdowinski, S., 2000. Distribution of slip at the northern Sumatra fault System, *J. geophys. Res.*, **105**(28), 327–341.
- Harvey, G.E., 1925. *History of Burma from the Earliest Times to 10 March 1824, The Beginning of the English Conquest*. Longmans, Green and Co., London, 415pp.
- Kamesh Raju, K.A., Ramprasad, T., Rao, P.S., Ramalingeswara Rao, B. & Varghese, J., 2004. New insights into the tectonic evolution of the Andaman basin, northeast Indian Ocean, *Earth planet. Sci. Lett.*, **221**(1–4), 145–162.
- Lacassin, R., Maluski, H., Leloup, P., Tapponnier, H.P., Hinthong, C., Siribhakdi, K., Chuaviroj, S. & Charoenravat, A., 1997. Tertiary diachronic extrusion and deformation of western Indochina: structural and  $^{40}\text{Ar}/^{39}\text{Ar}$  evidence from NW Thailand, *J. geophys. Res.*, **102**(B5), 10 013–10 037.
- Lacassin, R., Replumaz, A. & Hervé Leloup, P., 1998. Hairpin river loops and slip-sense inversion on southeast Asian strike-slip faults, *Geology*, **26**, 703–706.
- Le Dain, A.Y., Tapponnier, P. & Molnar, P., 1984. Active faulting and tectonics of Burma and surrounding regions, *J. geophys. Res.*, **89**(B1), 453–472.
- Lieberman, V., 1980. The Transfer of the Burmese Capital from Pegu to Ava, *J. R. Asiat. Soc.*, 64–83.
- Liu, Z. & Bird, P., 2008. Kinematic modelling of neotectonics in the Persia-Tibet-Burma orogen, *Geophys. J. Int.*, **172**(2), 779–797, doi:10.1111/j.1365-246X.2007.03640.x.
- McCaffrey, R., 1991. Slip vectors and stretching of the Sumatran fore arc, *Geology*, **19**, 881–884.
- Meade, B.J., 2007. Present-day kinematics at the India-Asia collision zone, *Geology*, **35**(1), 81–84.
- Milne, J., 1911. *A Catalogue of Destructive Earthquakes A. D. 7 to A. D. 1899*, BAAS, London.
- Morley, C.K., 2002. A tectonic model for the tertiary evolution of strike-slip faults and rift basins in SE Asia, *Tectonophysics*, **347**(4), 189–215.
- Myint Thein, Tint, K. & Aung, A.K., 1991. On the lateral displacement of the Sagaing fault, *Georeport*, **1**(1), 23–34.
- Ooi, K.G., 2004. *Southeast Asia: A Historical Encyclopedia from Angkor Wat to East Timor*, ABC-CLIO, Santa Barbara, CA, 1500pp.
- Pacheco, J.F. & Sykes, L.R., 1992. Seismic moment catalog of large shallow earthquakes, 1900 to 1989, *Bull. seism. Soc. Am.*, **82**, 1306–1349.
- Replumaz, A., 1999. Reconstruction de la zone de collision Inde-Asie – Etude centrée sur l’Indochine. *PhD thesis*, Université Paris 7-IPG, Paris.
- Saw Htwe Zaw, 2006. Hazard assessment in Multi-hazard Design, in *Symp. Tectonics, Seismotectonics, and Earthquake Hazard Mitigation and Management of Myanmar*, Yangon, Abstract.
- Schwartz, D. & Coppersmith, K., 1984. Fault behavior and characteristic earthquakes: examples from the Wasatch and San Andreas Fault Zones, *J. geophys. Res.*, **89**(B7), 5681–5698.
- Sieh, K., 1996. The repetition of large-earthquake ruptures, *Proc. Natl. Acad. Sci.*, **93**(9), 3764–3771.
- Sieh, K. & Natawidjaja, D., 2000. Neotectonics of the Sumatran fault, Indonesia, *J. geophys. Res.*, **105**, 28 295–28 326.
- Socquet, A., Vigny, C., Chamot-Rooke, N., Simons, W., Rangin, C. & Ambrosius, B., 2006. India and Sunda plates motion and deformation along their boundary in Myanmar determined by GPS, *J. geophys. Res.*, **111**, B05406, doi:10.1029/2005JB003877.
- Sokolov, V. & Wald, D.J., 2002. Instrumental intensity distribution for the Hector Mine, California, and the Chi-Chi, Taiwan, earthquakes: comparison of two methods, *Bull. seism. Soc. Am.*, **92**, 2145–2162.
- Tapponnier, P., Peltzer, G., Le Dain, A.Y., Armijo, R. & Cobbold, P., 1982. Propagating extrusion tectonics in Asia: new insights from simple experiments with plasticine, *Geology*, **10**, 611–616.
- Thawbita. 1976. Chronology—earthquakes of Burma, *J. Burm. Res. Soc.*, **59.1–2**, 97–99.
- Tsutsumi, H. & Sato, T., 2009. Tectonic Geomorphology of the Southernmost Sagaing Fault and Surface Rupture Associated with the May 1930 Pegu (Bago) Earthquake, Myanmar, *Bull. seism. Soc. Am.*, **99**, 2155–2168.
- U Kala. *Maha-ya-zawin-gyi, 1961-ed.* Vol. 3, Hsaya U Kin So, Rangoon (in Burmese).
- Vigny, C., Socquet, A., Rangin, C., Chamot-Rooke, N., Pubellier, M., Bouin, M.N., Bertrand, G. & Becker, M., 2003. Present-day crustal deformation around Sagaing fault, Myanmar, *J. geophys. Res.*, **108**(B11), 2533, doi:10.1029/2002JB001999.
- Wells, D.L. & Coppersmith, K.J., 1994. New empirical relationships among magnitude, rupture length, rupture width, rupture area, and surface displacement, *Bull. seism. Soc. Am.*, **84**, 974–1002.
- Win Swe, 1970. Rift-features at the Sagaing-Tagaung ridge, in *Proc. 5th Burma Research Congress*, Rangoon.
- Win Swe, 2006. Earthquake hazard potentials in Myanmar: a science to public welfare outlook, in *Symp. Tectonics, Seismotectonics, and Earthquake Hazard Mitigation and Management of Myanmar*, Yangon, Abstract.
- Wood, H.O. & Neumann, F., 1931. Modified Mercalli intensity scale of 1931, *Bull. seism. Soc. Am.*, **21**, 277–283.
- Yeats, R.S., Sieh, K.E. & Allen, C.R., 1997. *The Geology of Earthquakes*, Oxford Press, New York, NY, 568pp.

## SUPPORTING INFORMATION

Additional Supporting Information may be found in the online version of this article:

**Table S1.** Stories of the May 1930 earthquake from local villagers near the city of Bago (Pegu).

**Table S2.** Field photographs of small offsets along the Sagaing fault.

**Table S3.** Original description and English translation of the temporary palace near the Payagyi pagoda from U Kala’s Maha-ya-zawin-gyi (‘Great Chronicle’).

Please note: Wiley-Blackwell are not responsible for the content or functionality of any supporting materials supplied by the authors. Any queries (other than missing material) should be directed to the corresponding author for the article.